Journal of Computational Physics 229 (2010) 7180–7190

Contents lists available at ScienceDirect

Journal of Computational Physics

journal homepage: www.elsevier.com/locate/jcp

Generalized conservative approximations of split convective derivative operators

Sergio Pirozzoli *

Università degli Studi di Roma "La Sapienza", Dipartimento di Meccanica e Aeronautica, Via Eudossiana 18, 00184 Roma, Italy

ARTICLE INFO

Article history:
Received 27 January 2010
Received in revised form 21 April 2010
Accepted 4 June 2010
Available online 17 June 2010

Keywords:
Finite difference schemes
Compressible flows
Energy conservation
Split convective operators

ABSTRACT

We propose a strategy to design locally conservative finite-difference approximations of convective derivatives for shock-free compressible flows with arbitrary order of accuracy, that generalizes the approach of Ducros et al. (2000) [1], and that can be applied as a building block of low-dissipative, hybrid shock-capturing methods. The approximations stem from application of standard central difference formulas to split forms of the convective terms in the compressible Euler equations, which guarantee strong numerical stability and (near) energy preservation in the inviscid limit. A convenient implementation of the high-order fluxes is suggested, which guarantees improved computational efficiency over existing methods. Numerical tests performed for isotropic turbulence at zero viscosity show stability of schemes with order of accuracy up to ten, and effectiveness of convective splitting of Kennedy and Gruber (2008) [2] in providing extra stability in the presence of strong density variations. Numerical simulations of compressible turbulent boundary layer flow indicate suitability of the method for non-uniform grids, and overall support superior computational efficiency of high-order schemes.

1. Introduction

It is well known that, even in the absence of shock waves, straightforward central finite-difference approximations of fluid flow equations exhibit instability when used at zero (or very small) viscosity, owing to accumulation of aliasing errors resulting from discrete evaluation of the nonlinear convective terms [3]. Such deficiency can also be traced back to failure to discretely preserve (even approximately) quadratic invariants associated with the conservation equations [4,5]. For example, in the case of the Euler equations, kinetic energy is conserved in the incompressible limit in unbounded (or periodic) domains. Several attempts have been made over the years to develop numerical methods for the incompressible and compressible flow equations that replicate quadratic conservation properties in discrete sense. Most of the attempts appeared so far are loosely based on the idea of recasting the convective derivatives in 'skew-symmetric' split form, with the objective to minimize the aliasing error over other (analytically equivalent) forms [6], and to develop kinetic energy-consistent methods in the incompressible [7] and in the compressible case [8]. Alternative strategies to enforce kinetic energy preservation in the finite-volume framework without using splitting of the convective terms have been presented by Jameson [9], Subbareddy and Candler [10]. While use of the split form of convective derivatives generally guarantees good stability properties, the resulting discrete approximations cannot be generally cast in locally conservative form, i.e. as the difference of numerical fluxes at successive intermediate nodes. Local conservation guarantees discrete global conservation of the linear invariants (e.g. total mass, momentum and energy) through the telescopic property, and, most important, guarantees that the

* Tel.: +39 06 44585202; fax: +39 06 4881759.
E-mail address: sergio.pirozzoli@uniroma1.it.

0021-9991/$ - see front matter © 2010 Elsevier Inc. All rights reserved.
doi:10.1016/j.jcp.2010.06.006

Lax–Wendroff theorem [11] holds, ensuring convergence to a weak solution (provided the approximation itself converges). Such property is extremely useful if the scheme has to be used as a building block of hybrid shock-capturing algorithms, as shown by Larsson et al. [12], Johnsen et al. [13]. However, in that case, some artificial viscosity must be provided to inhibit the onset of Gibbs oscillations and guarantee convergence to the physically relevant entropy solution. Ducros et al. [1] first showed that (both in the finite-difference and in the finite-volume framework) numerical fluxes for convective terms in split form can be found for explicit central approximations of derivatives with accuracy order up to six. Those authors were able to confirm the stabilizing properties of convective splitting for various test cases, including steady and unsteady simulations.

The main objective of the present paper is to extend the analysis of Ducros et al. [1], and show that locally conservative finite-difference approximations of split convective derivatives can be designed with arbitrary order of accuracy. More important yet, we will show that the discrete approximations here proposed are substantially less computationally expensive than the straightforward application of difference formulas to convective derivatives in split form. This issue is of great practical importance, since incorporation of the present numerical fluxes into existing compressible flows solvers is extremely simple and cost-effective.

The paper is organized as follows: in Section 2 we derive formulas for numerical fluxes of arbitrary order of accuracy; in Section 3 we present numerical simulations of isotropic turbulence at infinite Reynolds number and of turbulent compressible boundary layer flow. Concluding remarks are given in Section 4.

2. Conservative formulation of split convective terms

We look for accurate and stable approximations of convective derivatives of the type encountered in the compressible Navier–Stokes equations, i.e.

$$\frac{\partial \rho u_k \varphi}{\partial x_k}, \tag{1}$$

where φ stands for a generic transported scalar property, being unity for the continuity equation, u_i ($i = 1,2,3$) for the momentum equation, $H = \gamma/(\gamma-1)p/\rho + u^2/2$ for the total energy equation. Assuming for the sake of the analysis one space dimension, and an equally spaced grid with nodes $x_j = j \cdot h$, we look for conservative finite-difference approximations of the type

$$\left.\frac{\partial \rho u \varphi}{\partial x}\right|_{x=x_j} \approx \frac{1}{h}\left(\hat{f}_{j+1/2} - \hat{f}_{j-1/2}\right), \tag{2}$$

where $\hat{f}_{j+1/2}$ is the numerical flux.

The split form of convective derivatives is obtained expanding the left-hand-side of Eq. (2) as either

$$\frac{\partial \rho u \varphi}{\partial x} = \frac{1}{2}\frac{\partial \rho u \varphi}{\partial x} + \frac{1}{2}\varphi\frac{\partial \rho u}{\partial x} + \frac{1}{2}\rho u\frac{\partial \varphi}{\partial x}, \tag{3}$$

or

$$\frac{\partial \rho u \varphi}{\partial x} = \frac{1}{2}\frac{\partial \rho u \varphi}{\partial x} + \frac{1}{2}u\frac{\partial \rho \varphi}{\partial x} + \frac{1}{2}\rho\varphi\frac{\partial u}{\partial x}. \tag{4}$$

It is worthwhile mentioning that, although the split convective forms (3) (introduced by Feiereisen et al. [14], and referred in the following as FE-SF) and (4) (introduced by Blaisdell et al. [15], and referred to as BL-SF), are often labeled as 'skew-symmetric', this is not strictly correct in mathematical terms, since the internal product of the corresponding differential operators with φ is not identically zero upon integration by parts, and therefore the integral of $\rho\varphi^2$ (i.e. the generalized energy) is not preserved in time. In this respect we note [16] that energy consistency at the semi-discrete is only guaranteed when both the continuity and the momentum equations are split according to (3), whereas the stabilization properties of the split form (4) derive from minimization of the aliasing error [15]. Split forms of the convective operators that are skew-symmetric in strict sense have been recently introduced by Morinishi [8].

Replacing the continuous derivative operators in (3) and (4) with their finite-difference counterparts yields

$$\left.\frac{\partial fg}{\partial x}\right|_{x=x_j} \approx D_S(fg)_j \equiv \frac{1}{2}D(fg)_j + \frac{1}{2}f_j Dg_j + \frac{1}{2}g_j Df_j, \tag{5}$$

where D_S denotes the discrete approximation of the split convective derivative, Df_j stands for the discrete approximation of the first derivative of f at node x_j, and ($f = \rho u, g = \varphi$) or ($f = \rho\varphi$, $g = u$) in the case of the split form (3) or (4), respectively. Standard central difference approximations of the first derivative operator will be considered here,

$$Df_j = \sum_{\ell=1}^{L} a_\ell D^\ell f_j, \quad D^\ell f_j = \frac{1}{h}(f_{j+\ell} - f_{j-\ell}), \tag{6}$$

where the coefficients a_ℓ are obtained by requiring either maximum formal order of accuracy of the approximation (i.e. $2L$), or that the discrete phase velocity approximates as closely as possible the exact one over an extended range of wavenumbers, yielding the class of the dispersion-relation-preserving (DRP) schemes [17].

Ducros et al. [1] showed that, for $L \leqslant 3$, insertion of (6) into (5) allows to cast the resulting convective derivative approximation in conservation form. In the simplest case $L = 1$, corresponding to a second-order approximation, one easily obtains

$$\hat{f}_{j+1/2} = \frac{1}{4}(f_j + f_{j+1})(g_j + g_{j+1}), \tag{7}$$

whereas a conservative approximation of the convective form (2) would yield

$$\hat{f}_{j+1/2} = \frac{1}{2}(f_j g_j + f_{j+1} g_{j+1}). \tag{8}$$

Explicit formulas for the numerical flux were also reported for $L = 2, 3$ in the original reference [1], corresponding to fourth- and sixth-order approximations, respectively.

In the following we show that explicit formulas for the numerical flux do exist for arbitrary L, and suggest an efficient implementation strategy. Indeed, considering a single term (D^ℓ) in the expansion (6), insertion into (5) yields, after simple developments

$$D_S^\ell(fg)_j = \frac{1}{2} D^\ell(fg)_j + \frac{1}{2} f_j D^\ell g_j + \frac{1}{2} g_j D^\ell f_j = \frac{2}{h}\left((\widetilde{f,g})_{j,\ell} - (\widetilde{f,g})_{j-\ell,\ell}\right), \tag{9}$$

where

$$\left(\widetilde{f,g}\right)_{j,l} = \frac{1}{4}(f_j + f_{j+\ell})(g_j + g_{j+\ell}), \tag{10}$$

is a two-point, two-variable discrete averaging operator. Note that Eq. (9) is not automatically written in conservation form, but it can be manipulated by summing and subtracting the term $\sum_{m=1}^{\ell-1}(\widetilde{f,g})_{j-m,\ell}$, to arrive to a locally conservative formulation

$$D_S^\ell(fg)_j = \frac{1}{h}\left(\hat{f}^\ell_{j+1/2} - \hat{f}^\ell_{j-1/2}\right), \quad \hat{f}^\ell_{j+1/2} = 2\sum_{m=0}^{\ell-1}(\widetilde{f,g})_{j-m,\ell}. \tag{11}$$

The overall numerical flux is then obtained by re-assembling the partial fluxes (11) as in (6),

$$\hat{f}_{j+1/2} = \sum_{\ell=1}^{L} a_\ell \hat{f}^\ell_{j+1/2}, \tag{12}$$

thus obtaining

$$\hat{f}_{j+1/2} = 2\sum_{\ell=1}^{L} a_\ell \sum_{m=0}^{\ell-1}(\widetilde{\rho u,\varphi})_{j-m,\ell}, \tag{13}$$

for the FE-SF split form, and

$$\hat{f}_{j+1/2} = 2\sum_{\ell=1}^{L} a_\ell \sum_{m=0}^{\ell-1}(\widetilde{\rho\varphi,u})_{j-m,\ell}, \tag{14}$$

for the BL-SF split form. It can be shown that the same formulas presented by Ducros et al. [1] are recovered from Eq. (14) for $L \leqslant 3$, using the values of the coefficients a_ℓ that maximize formal order of accuracy. We note that, besides providing explicit formulas for numerical fluxes with arbitrary order of accuracy, Eqs. (13) and (14) also allow use of DRP-type derivative discretizations, that may prove useful for flows in which wave propagation phenomena are important.

Kennedy and Gruber [2] suggested that additional robustness for flows with strong density variations can be gained by fully expanding the triple products that appear in (1), yielding the generalized split form

$$\frac{\partial \rho u\varphi}{\partial x} = \alpha\frac{\partial \rho u\varphi}{\partial x} + \beta\left(u\frac{\partial \rho\varphi}{\partial x} + \rho\frac{\partial u\varphi}{\partial x} + \varphi\frac{\partial \rho u}{\partial x}\right) + (1-\alpha-2\beta)\left(\rho u\frac{\partial \varphi}{\partial x} + \rho\varphi\frac{\partial u}{\partial x} + u\varphi\frac{\partial \rho}{\partial x}\right), \tag{15}$$

hereafter referred to as KG-SF. We have found that conservative approximations of the split form (15) can be recovered only under particular circumstances. Specifically, if $\alpha = \beta = 1/4$, following the same approach as for the 'standard' split formulations, we obtain

$$\hat{f}_{j+1/2} = 2\sum_{\ell=1}^{L} a_\ell \sum_{m=0}^{\ell-1}(\widetilde{\rho,u,\varphi})_{j-m,\ell}, \tag{16}$$

where the two-point, three-variable discrete averaging operator is defined as

$$(\widetilde{f,g,h})_{j,\ell} = \frac{1}{8}(f_j + f_{j+\ell})(g_j + g_{j+\ell})(h_j + h_{j+\ell}). \tag{17}$$

Comparison of this form of the numerical flux with the FE-SF and BL-SF split formulations shows that in this case the effect of density variation is taken into account separately from the other two variables, and in this sense we will also refer to the KG-

SF splitting, as well as to the conservative approximation (16), as 'density-weighted'. As for the standard FE-SF split form, one can easily prove that the KG-SF form (15) (with $\alpha = \beta = 1/4$) yields semi-discrete preservation of kinetic energy when applied to both the continuity and momentum equations.

It is important to note that the approximations (13), (14) and (16) can be efficiently implemented in a numerical code by preliminarily evaluating and storing the averages (10) and (17), for all j, $\ell \leqslant L$, and performing the linear combinations involved in the formulas in a second step. The number of floating point operations (sums and products) per grid point needed to evaluate a single convective derivative has been estimated for the various approximations considered so far, as explained in Appendix A. The direct finite-difference approximation of the convective derivative (1), denoted as D-CONV, requires $2 + 2L$ operations per node; straightforward application of the discrete derivative operator (6) to the FE-SF and BL-SF split forms (the resulting schemes are denoted as D-FE-SF and D-BL-SF, respectively), requires $6 + 6L$ operations; the approximation obtained applying (6) to the KG-SF split form (denoted as D-KG-SF) requires $20 + 14L$ floating point operations. With regard to the conservative formulations of the split convective forms, the schemes defined by the numerical fluxes (13) or (14) (denoted as C-FE-SF and C-BL-SF, respectively), require $2 + 7/2L + L^2/2$ operations; and the density-weighted approximation with numerical flux given by (16) (denoted as C-KG-SF) requires $1 + 9/2L + L^2/2$ operations. These cost estimates are displayed in Fig. 1, as a function of the stencil width (L). In the same figure we also report for reference purposes the cost incurred with direct application of the conservative formulas of Ducros et al. [1]. Although the computational cost grows quadratically with L for the conservative approximations, their cost is usually less than for the corresponding non-conservative formulations, while being entirely equivalent. Specifically, the C-FE-SF and C-BL-SF schemes are less CPU-intensive than their non-conservative counterpart for $L \leqslant 6$, whereas C-KG-SF is faster than KG-SF for $L \leqslant 18$. Furthermore, the present implementation is found to be substantially more efficient than the original conservative formulation of Ducros et al. [1]. Finally, one should note that the C-KG-SF scheme is only marginally more expensive than C-FE-SF and C-BL-SF. These estimates are consistent with the CPU time actually measured in numerical simulations, as also reported in Appendix A.

3. Numerical tests

3.1. Euler turbulence

To test the robustness of conservative approximations here proposed we have performed a series of numerical simulations of (unforced) isotropic compressible turbulence in a $(2\pi)^3$ periodic box at zero viscosity, as proposed by Honein and Moin [16]. The Euler equations are solved in their standard form, including the conservation equations of mass, momentum, and total energy. Time integration is performed by means of the third-order TVD Runge–Kutta scheme of Shu and Osher [18], that is widely used in compressible flow solvers, with CFL number set to unity. The calculations are initialized with a field of synthetic isotropic solenoidal turbulence with assigned wavenumber spectrum

$$E(k) = A(k/k_0)^4 \exp[-2(k/k_0)^2], \tag{18}$$

peaking at $k_0 = 6$. The constant A is adjusted in such a way that the initial turbulent Mach number $M_t = u_{\mathrm{r.m.s.}}/\bar{c}$ (where the prime indicates the r.m.s. value, and $\bar{c}$ is the mean speed of sound) is set to a desired value. Fluctuations of temperature and density are initially set to zero. Under such conditions an equipartition k^2 energy spectrum quickly develops [19]. The large energy content at the highest wavenumbers resolved on the computational grid poses a significant challenge to a numerical algorithm, leading to nonlinear instability in the absence of mechanisms to control aliasing errors.

The results of a series of calculations performed on a 32^3 (uniformly spaced) grid, for initial turbulent Mach number $M_{t0} = 0.07$ and $M_{t0} = 0.3$ are reported in Figs. 2 and 3, respectively. Data are shown for schemes with order of accuracy (corresponding to $2L$) up to 10. The results obtained with CONV schemes are not displayed in the figures, since they invariably lead to divergence of the solution on a time scale faster than one eddy turnover time for any order of accuracy.

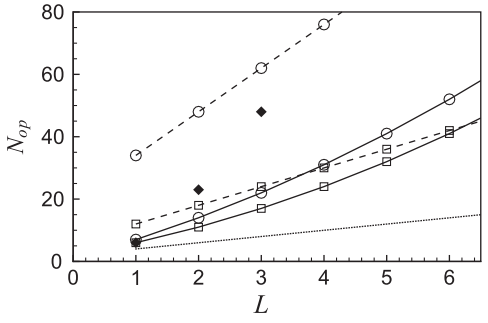

Fig. 1. Nominal cost (floating point operations/node) for convective derivative approximations with different stencil width. Dotted lines: baseline convective approximation (D-CONV); dashed lines: standard (non-conservative) approximation of split convective derivatives (D-); solid lines: conservative approximation of split convective derivatives (C-); square symbols: standard split forms FE-SF and BL-SF; circles: density-weighted split form (KG-SF); diamonds: conservative formulation of Ducros et al. [1].

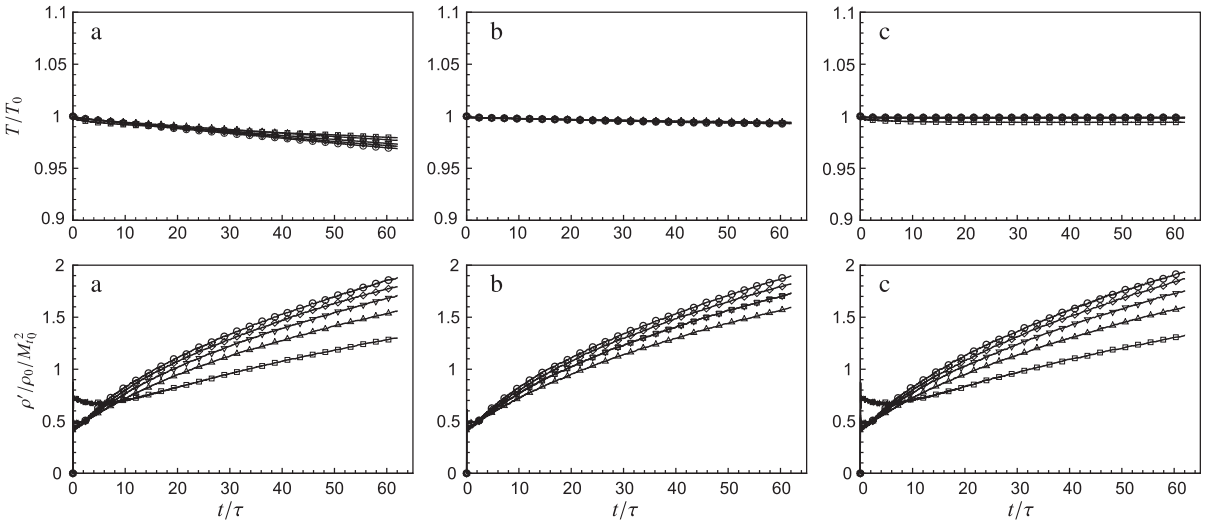

Fig. 2. Time evolution of total kinetic energy and r.m.s. density fluctuations for isotropic turbulence at zero viscosity ($M_{t0} = 0.07$). τ is the eddy turnover time. (a) C-BL-SF scheme; (b) C-FE-SF scheme; (c) C-KG-SF scheme. Symbols: □, $L = 1$; △, $L = 2$; ▽, $L = 3$; ◇, $L = 4$; ○, $L = 5$.

The low Mach number test case is identical to that considered by Honein and Moin [16], who showed that the 'exact' solution (computed by means of a de-aliased spectral method), has nearly constant total kinetic energy ($T = \int \rho u^2 \, dV$), and the r.m.s. density levels off to $\rho'/\rho_0/M_{t_0}^2 \approx 0.35$, after an initial transient. Overall, schemes based on convective splitting do a good job in preserving the initial kinetic energy, although they exhibit spurious drift of density fluctuations over long times (not leading to divergence yet). This observation is more true for the higher-order schemes, that preserve kinetic energy quite accurately, but exhibit excessive density fluctuations in the long run. On the other hand, second-order schemes show substantial error in kinetic energy preservation and an odd initial transient, but also reduced growth of density fluctuations. As expected, clear advantage in terms of energy preservation is observed for the C-FE-SF and C-KG-SF formulations, that yield kinetic energy variations of 0.6% at most, over the monitored time interval.

Clear advantage of the density-weighted formulation is found in the simulations at $M_{t0} = 0.3$, for which compressibility plays a significant role. In this case energy conservation is not to be expected, since exchanges between kinetic and internal energy modes are substantial. The results shown in Fig. 3 show that this is indeed the case. For this test case the standard split forms BL-SF and FE-SF lead to divergence of the numerical solution, whereas the density-weighted formulation seems to have a strong stabilizing effect, even though significant density drift is observed over long times. In this respect, it seems that the fourth-order version of the C-KG-SF scheme (corresponding to $L = 2$) is capable to force the system towards a (nearly) statistically steady asymptotic state.

We finally note that better results in physical terms can be obtained using schemes that exactly preserve energy in their fully discrete formulation (see, e.g. [10]), or replacing the total energy equation with the internal energy or the entropy equations [16], or using suitable time integration schemes. However, such features are rather difficult to incorporate in existing compressible flow codes, and are not addressed here, since our primary intent is to test robustness of the method.

3.2. DNS of compressible boundary layer

To challenge the capability of the present class of conservative schemes to cope with more realistic flow cases, and in particular with non-uniform meshes, we have performed the direct numerical simulation (DNS) of a spatially-developing compressible turbulent boundary layer at $M_\infty = 2$, using a set-up very similar to that described in Pirozzoli et al. [22]. To summarize, inlet turbulence is enforced using a recycling/rescaling procedure, periodicity is used in the spanwise direction, purely nonreflecting boundary conditions are used at the outflow and at the top boundary, whereas unsteady characteristic boundary conditions with fixed temperature [23] are specified at the bottom wall. The computational domain was selected to be sufficiently wide ($L_z/\delta_{in} = 5$, where δ_{in} is the boundary layer thickness at the inflow) to avoid the development of spurious correlations in the spanwise direction. The convective fluxes are discretized by means of the sixth-order conservative density-weighted split scheme (C-KG-SF). As pointed out by Ducros et al. [1], a fully conservative finite-difference discretization using the split form of the convective derivatives is not possible on a mesh with variable spacing. We have then followed the customary approach of using the chain rule to approximate spatial derivatives, and used conservative discretization in computational space, that proves to be very effective in practice. With regard to the viscous terms, we have used a non-conservative discretization, whereby the Laplacian operators are isolated, and both first and second derivatives are discretized with sixth-order central approximations. This approach effectively guarantees that the highest resolvable

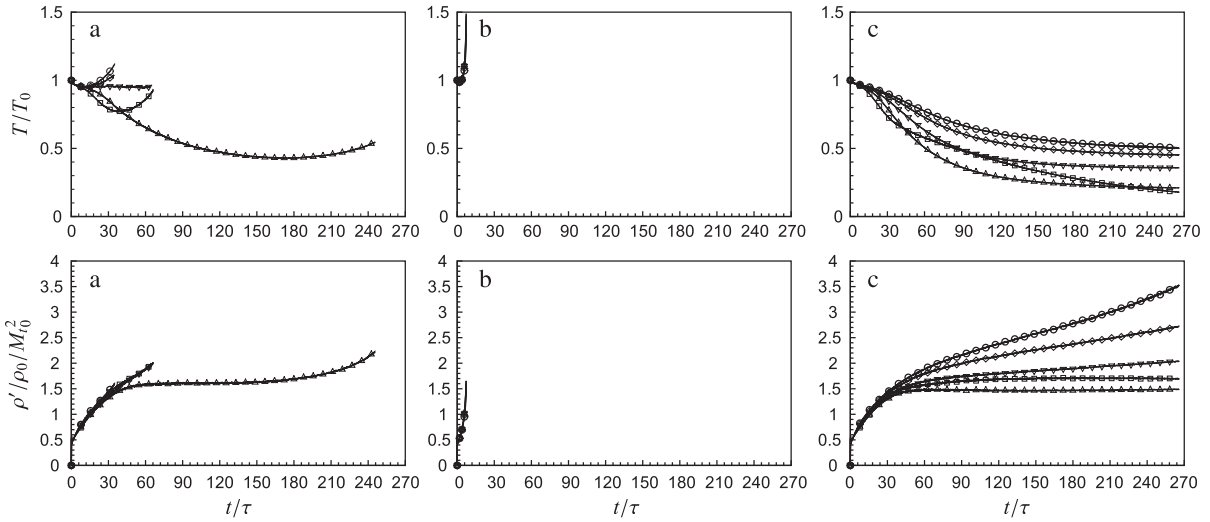

Fig. 3. Time evolution of total kinetic energy and r.m.s. density fluctuations for isotropic turbulence at zero viscosity ($M_{t0} = 0.3$). τ is the eddy turnover time. (a) C-BL-SF scheme; (b) C-FE-SF scheme; (c) C-KG-SF scheme. Symbols: □, $L = 1$; △, $L = 2$; ▽, $L = 3$; ◇, $L = 4$; ○, $L = 5$.

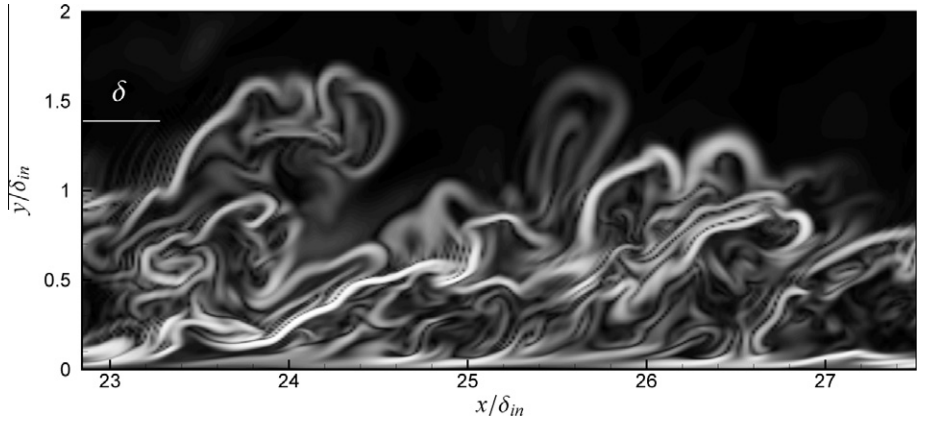

Fig. 4. Instantaneous Schlieren-like visualization of (portion of) boundary layer in x–y plane. Sixty-four levels of the variable $\exp(-0.5|\nabla\rho|\delta_{in}/\rho_\infty)$ are shown from *0* to *1*, colors scale white to black. δ is the local boundary layer thickness; δ_{in} is the inflow boundary layer thickness (i.e. at $x = 0$).

wavenumbers undergo accurate viscous damping [24]. Time integration is performed by means of a standard fourth-order Runge–Kutta algorithm in this case.

At the station selected for collecting the flow statistics ($x/\delta_{in} = 25$), the Reynolds number based on the momentum thickness is $Re_\theta = 1573$, and the friction Reynolds number is $\delta^+ = 356$. The computational grid has uniform spacing in the streamwise and spanwise directions (in terms of wall units, $\Delta x^+ \approx \Delta z^+ \approx 4.5$), and it is stretched in the wall-normal direction according to a hyperbolic sine distribution. The first point off the wall lies at a distance $\Delta y_w^+ = 0.54$, and the grid spacing at the edge of the boundary layer is $\Delta y_\delta^+ = 6.1$. Exploratory calculations have shown that even with this very fine grid the D-CONV scheme leads to numerical divergence in short time.

A small slice of the flow field in a wall-normal/longitudinal plane is shown in Fig. 4, in terms of a Schlieren-like representation, whereby the field of $\exp(-0.5|\nabla\rho|\delta_{in}/\rho_\infty)$ is reported to emphasize small density variations. Assuming that density can in a first approximation interpreted as a passive tracer in a weakly compressible flow, the figure highlights the occurrence of density fronts in the outer part of the boundary layer (associated with the outer layer 'bulges'), that separate the inner turbulence from the outside essentially irrotational main flow. Some ringing is observed near the edge of the boundary layer, where the extremely sharp density gradients cannot be fully resolved.

The flow statistics, in terms of the mean velocity distribution and of the velocity fluctuation intensities are reported in Fig. 5, at a station where boundary layer turbulence is fully developed. Note that, to compare to reference incompressible experimental and DNS data, the Van Driest effective velocity is considered,

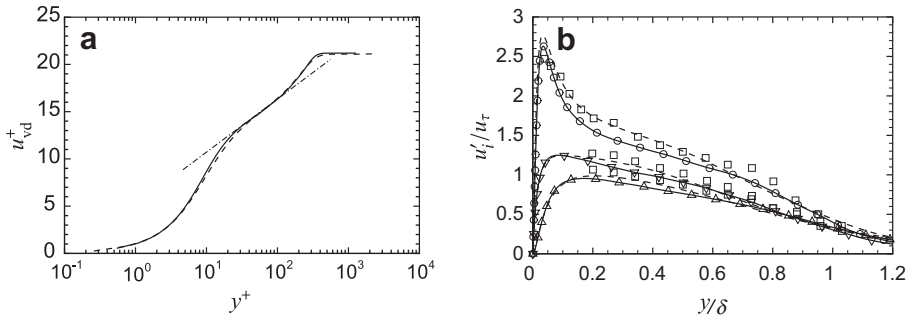

Fig. 5. Distributions of: (a) Van Driest transformed mean streamwise velocity: (b) r.m.s. velocity fluctuations. Solid lines, present DNS; dashed lines: DNS of Wu and Moin [20]; chained line, $u^+_{vd} = 5.1 + 1/0.41 \log y^+$. Symbols: ○, streamwise component; △, wall-normal component; ▽, spanwise component; □, experiments of Erm and Joubert [21].

Table 1
Grid parameters for turbulent boundary layer simulations.

Grid	Δx^+	Δz^+	Δy^+_w	Δy^+_δ
DNS	4.4	4.5	0.54	6.1
A	19.0	10.5	0.88	15.7
B	28.1	15.9	0.94	28.1
C	46.4	25.5	1.05	44.2

$$u_{vd} = \int_0^{\bar{u}} \left(\frac{\bar{\rho}}{\bar{\rho}_w}\right)^{1/2} d\bar{u}. \tag{19}$$

The distribution of the Van Driest velocity, reported in Fig. 5a, shows excellent collapse with the incompressible DNS data of Wu and Moin [20] (having $\delta^+ \approx 400$), highlighting the presence of a small logarithmic region. With regard to the statistics of velocity fluctuations, reported in Fig. 5b, very good agreement with DNS and experiments is observed for the transverse components, whereas the longitudinal component shows quantitative differences, especially in the inner layer, that are likely related to the effect of compressibility [25]. In this respect we mention that the maximum turbulence Mach number across the boundary layer is $M_t \approx$ 0.24, for which compressibility effects are expected to be small, but not negligible.

Additional simulations of the same test case have been performed on under-resolved grids to assess: (i) the effect of the type of convective splitting on robustness and accuracy; and (ii) the possible improvement of computational efficiency brought by high-order discretizations.

With regard to the first item, a series of calculations have been performed by applying the C-BL-SF, C-FE-SF, and C-KG-SF schemes (with $L = 3$) on a sequence of progressively coarsened grids having the same size as the DNS grid, and whose main parameters are listed in Table 1. The distributions of the computed r.m.s. streamwise velocity fluctuations and spanwise spectra (at $y^+ = 100$) are reported in Figs. 6 and 7, respectively. Fig. 6 shows a non-monotone trend of r.m.s. velocity with grid resolution, whereby marginally resolved grids (grid A) yield a decrease of the r.m.s. peak, whereas significantly under-resolved grids yield an increase of the near-wall peak, and loss of kinetic energy in the outer layer. Overall, different schemes yield similar results on the same grid, with a somewhat more accurate representation of the r.m.s. peak by the C-BL-SF scheme. With regard to robustness, we find that the C-FE-BL scheme is much less robust than the other ones, and leads to numerical divergence on grid C. Somewhat superior robustness of the C-KG-SF scheme over C-BL-SF has been observed for further coarsened grids (compared to grid C), on which however the flow statistics are very inaccurate. Similar considerations can be repeated for the velocity spectra of Fig. 7. In this case, under-resolution manifests itself in excessive energy transfer from the large to the small scales of motion, with subsequent energy pile-up. Marginal differences are found among different schemes, the C-BL-SF and C-KG-SF schemes yielding perhaps improved representation of the low wavenumbers.

The effect of the order of accuracy has been studied by monitoring the performance of the C-BL-SF scheme on grid A for various L. The main results of the study, in terms of r.m.s. velocity fluctuations and spectra, are reported in Fig. 8, where the data are compared with the full DNS results. The figure shows that the second-order version of the scheme (corresponding to $L = 1$) over-estimates the r.m.s. velocity peak, as well as the energy content at high wavenumbers. Schemes with order of accuracy greater or equal to six ($L \geqslant 3$) yield adequate representation of the velocity fluctuations in the outer layer, and a consistent improvement in the resolution of the higher spectral modes as L increases.

As proposed by Johnsen et al. [13], the comparison of spectra from under-resolved calculations and DNS, as reported in Fig. 8b, can be used to gauge the computational efficiency of numerical methods in practical turbulent flow computations. For that purpose, we define a spectral error as

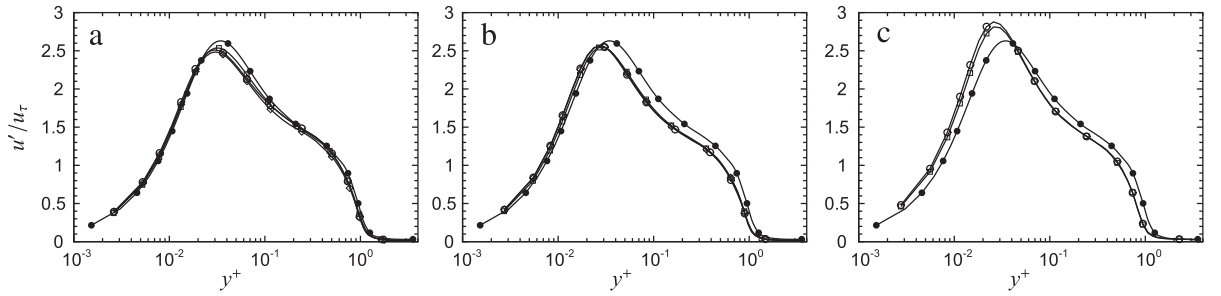

Fig. 6. Distributions of r.m.s. streamwise velocity fluctuations as a function of wall distance for under-resolved simulations (grids a, b, c). Symbols: •, DNS; □, C-BL-SF; ◇, C-FE-SF; ○, C-KG-SF.

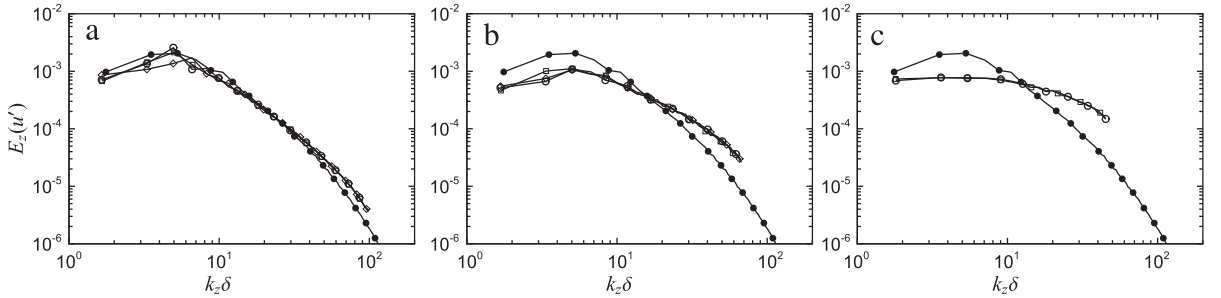

Fig. 7. Computed spanwise spectra of streamwise velocity fluctuations at $y^+ = 100$ for under-resolved simulations (grids a, b, c). Symbols: •, DNS; □, C-BL-SF; ◇, C-FE-SF; ○, C-KG-SF.

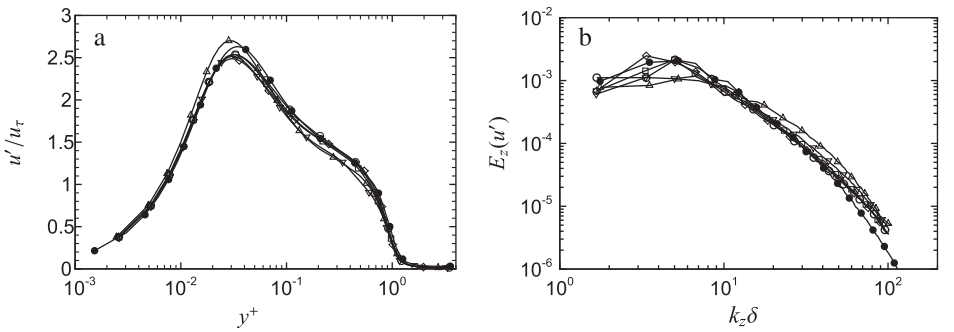

Fig. 8. Distributions of r.m.s. streamwise velocity fluctuations (a) and spanwise spectra of streamwise velocity fluctuations (b) for under-resolved simulations (grid A) with C-BL-SF schemes with different order of accuracy. Symbols: •, DNS; △, $L = 1$; ▽, $L = 2$; □, $L = 3$; ◇, $L = 4$; ○, $L = 5$.

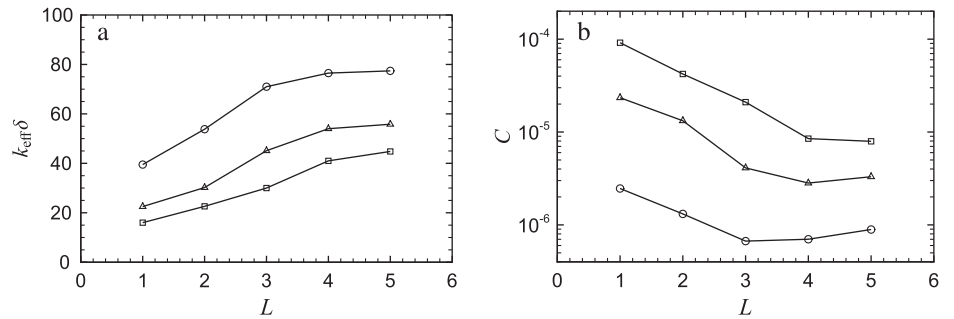

Fig. 9. Effective bandwidth (a) and computational cost (b) as a function of stencil half-width (L) for C-BL-SF scheme for various target errors. Symbols: □, $\bar{\varepsilon} = 0.25$; △, $\bar{\varepsilon} = 0.5$; ○, $\bar{\varepsilon} = 1$.

$$\varepsilon(k_z) = \frac{E_z(u';k_z)}{E_z^{\mathrm{DNS}}(u';k_z)} - 1, \tag{20}$$

and introduce an 'effective bandwidth' as the wavenumber (say k_{eff}) where the error first becomes larger than a prescribed threshold (say $\bar{\varepsilon}$). The effective bandwidths associated with the C-BL-SF scheme at various L are shown in Fig. 9, for target error levels $\bar{\varepsilon} = 0.25, 0.5, 1$. For that purpose, the first four Fourier modes in the spectra of Fig. 7 have been removed, since they more sensitively depend upon the details of the computational arrangement, as well as on the exact placement of the velocity probes (the probes used for spectral analysis are not placed at exactly the same height above the wall in the DNS and in the under-resolved calculations). As expected, Fig. 9 shows that the effective bandwidth increases with the order of accuracy. The computational cost incurred to attain a prescribed accuracy is then estimated assuming that: (i) the number of grid points required in each coordinate direction scales as $1/k_{\mathrm{eff}}$ (so as the number of time steps); (ii) the cost per unit node is given by the estimates of Appendix A. These assumptions result in the overall cost estimate $C = (2 + 7/2L + L^2/2)/k_{\mathrm{eff}}^4$, displayed in Fig. 9b. The figure shows that, in general terms, higher-order schemes yield superior computational efficiency, i.e. require less computational effort to achieve a given error level. However, the figure also suggest the occurrence of an 'optimal' order of accuracy, resulting from the competing effects of cost overhead and improvement in resolution in wavenumber space, that is a function of the target accuracy level. Specifically, schemes with high-order of accuracy (up to 10) may be desirable if (relatively) strict error tolerances are set, whereas lower order schemes (down to six) do a good job if (relatively) rough approximations as sought for.

4. Conclusions

A general framework for the design of conservative quasi-skew-symmetric schemes in shock-free flows has been established. The study proves that convective derivatives cast in split form, and discretized with explicit finite-difference central approximations with arbitrary accuracy can be properly recast in a locally conservative form, and therefore yield automatic conservation of total mass, momentum, and energy. This property is particularly important if the schemes are to be used as building blocks of hybrid shock-capturing algorithms, since the Lax–Wendroff theorem applies. Apparently, a conservative formulation cannot be arrived at if the explicit central difference operators are replaced with compact approximations. In that case, problems with conservation of linear invariants may be expected.

The specific conservative implementation proposed in the paper (as defined by the numerical fluxes (13), (14), (16)) guarantees significant improvement, in terms of computational efficiency, over straightforward discretization of split convective operators. The present strategy also provides additional freedom over existing formulations [1] to encompass more general convective splittings (such as the one proposed by Kennedy and Gruber [2]), as well as more general derivative approximations (e.g. DRP-type), which can be an advantage for calculations in which the far acoustic field is included.

Numerical experiments performed for Euler turbulence and for turbulent boundary layer flow show the robustness of split convective discretizations with order of accuracy up to 10, and confirm that, although local conservation cannot be proved on non-uniform grids, the algorithms work out very well in practice. The numerical experiments shows significant advantage of the BL-SF and KG-SF (and especially of the latter) split convective formulations in severely under-resolved calculations, when compressibility plays a significant role. Under-resolved boundary layer calculations also show the effectiveness of schemes with high-order of accuracy in producing an extended range of well-resolved wavenumbers, and the possible occurrence of an 'optimal' order of accuracy, that is dependent upon the prescribed error tolerance.

Acknowledgments

I am indebted to P. Orlandi for bringing to my attention energy-consistent approximations, and to M. Bernardini and S.K. Lele for comments on a preliminary version of the paper.

Appendix A. Computational efficiency estimates

The computational effort involved in the discrete approximations of the convective derivatives is here estimated by counting the overall number of floating point operations (f.p.o.), giving the same weight to sums and multiplications (no division operation is strictly necessary).

Referring to the standard form of the convective operator (1), its discrete approximation (D-CONV) reads $D\,(\rho u \varphi)_j$. The evaluation of the triple products at the grid nodes requires $2N$ multiplications (where N is the number of nodes), and the evaluation of the difference formulas (6) implies L multiplications and L sums per node (assuming the $1/h$ factor is absorbed into the a_ℓ), yielding a total of $2N(L+1)$ f.p.o.

With regard to the non-conservative discretization of the split convective derivatives (D-FE-SF and D-BL-SF) (5), the computational cost is estimated as follows: (i) pre-storage of f requires N multiplications; (ii) pre-storage of $f \cdot g$ requires N multiplications; (iii) the approximations of the derivatives of $f, g, f \cdot g$ according to (6) requires $3L$ multiplications and $3L$ sums per node; (iv) the right-hand-side of (5) can be evaluated at the cost of *2* sums and *2* multiplications per node. The total number of operations turns out to be $N(6 + 6L)$.

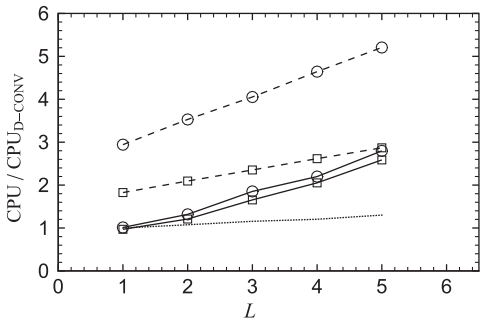

Fig. 10. Measured CPU time for Euler turbulence calculations (compared with CPU time for the second-order D-CONV scheme). Dashed lines: standard (non-conservative) approximation of split convective derivatives (D-); solid lines: conservative approximation of split convective derivatives (C-); square symbols: standard split forms (FE-SF and BL-SF); circles: density-weighted split form (KG-SF).

With regard to the conservative discretization of the split convective derivatives (C-FE-SF and C-BL-SF), we reason as follows: (i) pre-storage of f requires N multiplications; (ii) pre-storage of the averages (10) for all j, $\ell \leqslant L$ requires $2L$ sums and L multiplication per node (assuming the factor 1/4 is absorbed into the a_ℓ); (iii) evaluation of the linear combinations (13) or (14) requires $\ell - 1$ sums for each value of ℓ, and L multiplications, for a total of $\sum_{\ell=1}^{L}(1+\ell) = L(L+1)/2$ f.p.o. per node; (iv) the evaluation of the conservative formulas (2) requires N sums (again assuming the $1/h$ factor is absorbed in the a_ℓ). The overall number of f.p.o. is therefore $N(2 + 7/2L + L^2/2)$.

Similar reasonings can also be applied to deduce cost estimates for the density-weighted convective derivative approximations. Note that, since the derivatives are computed line-wise, there is no significant memory overhead associated with pre-storage of the averages (10).

As a check of the computational cost estimates, we have measured the CPU time required to perform the Euler turbulence simulations reported in Section 3.1. The results are reported in Fig. 10 (to be compared with Fig. 1), where all the CPU times are normalized with respect to the second-order D-CONV scheme, and the same nomenclature is used as for Fig. 1. Although additional operations are required by the Euler solver over the ones considered in the above cost estimates, the trend of the measured CPU times is similar to the expectations.

Sample routines including efficient implementation of conservative split derivatives for the compressible Euler equations are available by the author upon request.

References

[1] F. Ducros, F. Laporte, T. Soulères, V. Guinot, P. Moinat, B. Caruelle, High-order fluxes for conservative skew-symmetric-like schemes in structures meshes: application to compressible flows, J. Comput. Phys. 161 (2000) 114–139.
[2] C.A. Kennedy, A. Gruber, Reduced aliasing formulations of the convective terms within the Navier–Stokes equations, J. Comput. Phys. 227 (2008) 1676–1700.
[3] N.A. Phillips, An example of nonlinear computational instability, in: The Atmosphere and the Sea in Motion, Rockefeller Institute Press, Oxford University Press, 1959, pp. 501–504.
[4] D.K. Lilly, On the computational stability of numerical solutions of time-dependent non-linear geophysical fluid dynamics problems, J. Comput. Phys. 93 (1965) 11–26.
[5] P. Orlandi, Fluid Flow Phenomena: A Numerical Toolkit, Kluwer, Dordrecht, 2000.
[6] A.G. Kravchenko, P. Moin, On the effect of numerical errors in large eddy simulations of turbulent flows, J. Comput. Phys. 131 (1997) 310–322.
[7] Y. Morinishi, T.S. Lund, O.V. Vasiliev, P. Moin, Fully conservative higher order finite difference schemes for incompressible flow, J. Comput. Phys. 143 (1998) 90–124.
[8] Y. Morinishi, Skew-symmetric form of convective terms and fully conservative finite difference schemes for variable density low-Mach number flows, J. Comput. Phys. 229 (2010) 276–300.
[9] A. Jameson, Formulation of kinetic energy preserving conservative schemes for gas dynamics and direct numerical simulation of one-dimensional viscous compressible flow in a shock tube using entropy and kinetic energy preserving schemes, J. Sci. Comput. 34 (2008) 188–208.
[10] P.K. Subbareddy, G.V. Candler, A fully discrete, kinetic energy consistent finite-volume scheme for compressible flows, J. Comput. Phys. 228 (2009) 1347–1364.
[11] P.D. Lax, B. Wendroff, Systems of conservation laws, Comm. Pure Appl. Math. 13 (1960) 217–237.
[12] J. Larsson, S.K. Lele, P. Moin, Effect of numerical dissipation on the predicted spectra for compressible turbulence, Annu. Res. Briefs, Center for Turbulence Research, Stanford University, 2007.
[13] E. Johnsen, J. Larsson, A.V. Bhagatwala, W.H. Cabot, P. Moin, B.J. Olson, P.S. Rawat, S.K. Shankar, B. Sjgreen, H.C. Yee, X. Zhong, S.K. Lele, Assessment of high-resolution methods for numerical simulations of compressible turbulence with shock waves, J. Comput. Phys. 229 (2010) 1213–1237.
[14] W.J. Feiereisen, W.C. Reynolds, J.H. Ferziger, Numerical simulation of a compressible, homogeneous, turbulent shear flow, Report TF 13, Thermosci. Div., Mech. Eng., Stanford University, 1981.
[15] G.A. Blaisdell, E.T. Spyropoulos, J.H. Qin, The effect of the formulation of non-linear terms on aliasing errors in spectral methods, Appl. Numer. Math. 21 (1996) 207–219.
[16] A.E. Honein, P. Moin, Higher entropy conservation and numerical stability of compressible turbulence simulations, J. Comput. Phys. 201 (2004) 531–545.
[17] C.K.W. Tam, J.C. Webb, Dispersion-relation-preserving finite difference scheme for computational acoustics, J. Comput. Phys. 107 (1993) 262–281.
[18] C.-W. Shu, S. Osher, Efficient implementation of essentially non-oscillatory shock-capturing schemes II, J. Comput. Phys. 83 (1989) 32–78.
[19] R.H. Kraichnan, On the statistical mechanics of an adiabatically compressible fluid, J. Acoust. Soc. Am. 27 (1955) 438–441.

[20] X. Wu, P. Moin, Direct numerical simulation of turbulence in a nominally zero-pressure-gradient flat-plate boundary layer, J. Fluid Mech. 630 (2009) 5–41.
[21] L.P. Erm, J. Joubert, Low Reynolds number turbulent boundary layers, J. Fluid Mech. 230 (1991) 1–44.
[22] S. Pirozzoli, M. Bernardini, F. Grasso, Direct numerical simulation of transonic shock/boundary layer interaction under conditions of incipient separation, J. Fluid Mech., in press.
[23] T.S. Poinsot, S.K. Lele, Boundary conditions for direct simulations of compressible viscous flows, J. Comput. Phys. 101 (1992) 104–129.
[24] S.K. Lele, Compact finite difference schemes with spectral-like resolution, J. Comput. Phys. 103 (1992) 16–42.
[25] A.J. Smits, J.P. Dussauge, Turbulent Shear Layers in Supersonic Flow, American Institute of Physics, New York, 2006.